New Journal of Physics
The open access journal at the forefront of physics

Deutsche Physikalische Gesellschaft DPG IOP Institute of Physics

PAPER • OPEN ACCESS

Universal spin-glass behaviour in bulk $LaNiO_2$, $PrNiO_2$ and $NdNiO_2$

To cite this article: Hai Lin *et al* 2022 *New J. Phys.* **24** 013022

New Journal of Physics
The open access journal at the forefront of physics

Deutsche Physikalische Gesellschaft DPG
IOP Institute of Physics

Published in partnership with: Deutsche Physikalische Gesellschaft and the Institute of Physics

OPEN ACCESS

RECEIVED
13 October 2021

REVISED
1 December 2021

ACCEPTED FOR PUBLICATION
24 December 2021

PUBLISHED
13 January 2022

PAPER

Universal spin-glass behaviour in bulk $LaNiO_2$, $PrNiO_2$ and $NdNiO_2$

Hai Lin[1,*], **Dariusz Jakub Gawryluk**[2], **Yannick Maximilian Klein**[2], **Shangxiong Huangfu**[1], **Ekaterina Pomjakushina**[2], **Fabian von Rohr**[3] and **Andreas Schilling**[1]

[1] Department of Physics, University of Zürich, Winterthurerstrasse 190, CH-8057 Zürich, Switzerland
[2] Laboratory for Multiscale Materials Experiments (LMX), Paul Scherrer Institute (PSI), Forshungstrasse 111, CH-5232 Villigen, Switzerland
[3] Department of Chemistry, University of Zürich, Winterthurerstrasse 190, CH-8057 Zürich, Switzerland
[*] Author to whom any correspondence should be addressed.

E-mail: hailin@physik.uzh.ch

Keywords: spin glass, nickelate, magnetism, superconductivity

Abstract

Motivated by the recent discovery of superconductivity in infinite-layer nickelate thin films, we report on a synthesis and magnetization study on bulk samples of the parent compounds $RNiO_2$ (R = La, Pr, Nd). The frequency-dependent peaks of the alternating current magnetic susceptibility, along with remarkable memory effects, characterize spin-glass states. Furthermore, various phenomenological parameters via different spin glass models show strong similarity within these three compounds as well as with other rare-earth metal nickelates. The universal spin-glass behaviour distinguishes the nickelates from the parent compound $CaCuO_2$ of cuprate superconductors, which has the same crystal structure and d^9 electronic configuration but undergoes a long-range antiferromagnetic order. Our investigations may indicate a distinctly different nature of magnetism and superconductivity in the bulk nickelates than in the cuprates.

1. Introduction

The nickelates are widely believed to be promising candidates for unconventional superconductors because of their very similar structures and possibly related electronic states to the cuprates. Superconductivity was realized in nickelate thin films. $Nd_{1-x}Sr_xNiO_2$ films grown on $SrTiO_3$ were found to be superconducting with T_c = 9–15 K [1], and corresponding $Pr_{1-x}Sr_xNiO_2$ films with T_c = 7–12 K [2]. Very recently, Sr- and Ca-doped $LaNiO_2$ thin films [3, 4] have also been shown to be superconducting. These discoveries have aroused intensive research and discussions, but several open questions remain.

First, superconductivity is absent in bulk samples, e.g. in bulk $Nd_{1-x}Sr_xNiO_2$ [5, 6] and $Sm_{1-x}Sr_xNiO_2$ [7], and no signs of long-range magnetic orders have been observed. This discrepancy between non-superconducting bulk samples and superconducting thin films has not been well understood so far. Off-stoichiometry defects or chemical inhomogeneity in bulk samples are likely suspects to hamper superconductivity, while the role of the $SrTiO_3$ substrate has also been considered [8–11]. Strain effects have been frequently invoked to explain the occurrence of superconductivity in thin films [9, 12]. However, the 3% larger lattice constant along the c direction in thin films that must affect the Ni d_{z^2} orbital and is considered to be crucial for nickelate superconductivity [13], may be alternatively ascribed to the details of the film-growth process, in a similar way to $MgTi_2O_4$ films where a change of the out-of-plane lattice parameter alone can induce superconductivity [14]. Second, the parent phase $RNiO_2$ shows several differences from the isostructural parent compound $CaCuO_2$, which can be a high-temperature superconductor upon doping [15, 16]. Although $NdNiO_2$ and $CaCuO_2$ have the same infinite-layer structure and the same $3d^9$ configuration, $NdNiO_2$ is a conductor [17] (or a weak insulator [1, 5, 6, 17–19]) without any long-range magnetic order, whereas $CaCuO_2$ is an antiferromagnetic (AFM) Mott insulator [20]. The superconductivity in the nickelate may therefore be far away from the well-known scenario in

high-temperature superconductors, where AFM spin fluctuations have been suggested to act as the medium to promote superconductivity. More distinctions, such as a larger charge transfer gap and smaller AFM exchange energy have been found in experiments [21, 22] and theoretical calculations [23–27]. Moreover, the role of the 4*f* electrons of the *R* ions in RNiO$_2$ is still unknown. Theoretical calculations propose that the 4*f* electrons have an important influence on the electronic structure through 4*f*–5*d* interactions [28–30], although the doped LaNiO$_2$ thin films have recently also been shown to superconduct [3, 4].

A good starting point to clarify these questions would be to study the magnetism of the parent phases. The difficulty we face is to obtain bulk samples of RNiO$_2$, especially PrNiO$_2$, and to distinguish the intrinsic magnetism therein. In this work, we synthesized bulk LaNiO$_2$, PrNiO$_2$ and NdNiO$_2$ samples and systematically investigated their magnetic properties. We show that magnetic memory effects and frequency-dependent spin freezing peaks in alternating current (AC) magnetization reveal a universal spin-glass behaviour in RNiO$_2$.

2. Method

The synthesis of RNiO$_2$ (R = La, Pr, Nd) samples was conducted in two stages, according to the same procedure as in previous reports [5–7, 17, 31]. Here, we put an emphasis on bulk PrNiO$_2$, which is obtained for the first time up to our best knowledge. In the first stage, high-quality PrNiO$_3$ samples were grown under a high-pressure oxygen atmosphere [32]. In the second stage, the precursor PrNiO$_3$ samples were topochemically reduced by applying the following route, mixed with CaH$_2$, sealed in quartz tubes and heated at 270 °C for 40 h. Afterwards, the mixtures were washed by NH$_4$Cl in ethanol to remove the extra CaH$_2$ and Ca(OH)$_2$. The resulting black powders were PrNiO$_2$. LaNiO$_2$ and NdNiO$_2$ were synthesized in the same way. The pictures taken by a scanning electron microscope (SEM) indicate that all these samples consist of 1–5 μm sized particles, as shown in the insets in figure 1. Last but not least, the samples were stored in sealed centrifuge tubes and handled in the N$_2$ atmosphere in order to avoid degradation caused by water or oxygen in the air.

We made an elemental analysis with both energy-diffraction spectra (EDX) and thermal gravity (TG). The EDX measurements as well as the SEM pictures were performed on a Zeiss GeminiSEM 450 with a beam energy of 10 keV. The obtained atomic ratios were R:Ni = 1.01/1.04/1.02 for La/Pr/NdNiO$_2$, respectively. The TG analysis was done to determine the oxygen content in the respective oxides. Considering that the RNiO$_2$ samples would be totally reduced to R_2O$_3$ and Ni by H$_2$ in 700 °C, and by comparing precisely the mass before and after the reduction, the oxygen contents were deduced to 2.05/1.95/1.99 $\pm$ 0.04 for La/Pr/NdNiO$_2$, respectively. Altogether, the chemical composition of RNiO$_2$ we obtained is very close to the nominal compounds RNiO$_2$ within experimental resolution.

The x-ray diffraction (XRD) measurements were performed on a Bruker AXS D8 Advance diffractometer (Bruker AXS GmbH, Karlsruhe, Germany), equipped with a Ni-filtered Cu Kα radiation and a 1D LynxEye PSD detector. The Rietveld refinement analysis [33] of the diffraction patterns was performed with the package FULLPROF SUITE (version March-2019). All the magnetic measurements including the direct current (DC), AC magnetic susceptibility and memory effect, were performed in a magnetic properties measurement system (quantum design MPMS-3).

3. Results

We performed XRD measurements to characterize the crystal structures of the as-synthesized RNiO$_2$ samples. The corresponding data are shown in figure 1, together with refinements via the Rietveld method and the calculated Bragg peaks. As illustrated in figure 1(a), after extracting the apical oxygen in RNiO$_3$, the NiO$_2$-planes in RNiO$_2$ are separated by rare-earth metal ions layer by layer. The reduction might in principle be incomplete or introduce crystalline disorder or even destroy the NiO$_2$-planes into elemental Ni. However, the calculated curves fit well with the experimental ones, and all RNiO$_2$ compounds can be successfully refined as tetragonal phases with the same space group $P4/mmm$. These XRD results indicate that no significant distortions were introduced in the NiO$_2$-plane by the reduction, and the compounds can indeed be considered as the infinite-layer phase. The crystal parameters obtained from the Rietveld refinements are presented in table 1. The c-axis parameters of LaNiO$_2$, PrNiO$_2$ and NdNiO$_2$ are 3.363 Å, 3.285 Å and 3.279 Å, respectively. They are close to the reported values for bulk samples [5, 17, 31, 34, 35], but 3% smaller than in thin films [1, 2]. The different c values in our samples can be simply attributed to the different radii of rare-earth metal ion for coordination number $N = 8$ that $r(La^{3+}) = 1.15$ Å, $r(Pr^{3+}) = 1.11$ Å and $r(Nd^{3+}) = 1.10$ Å [36].

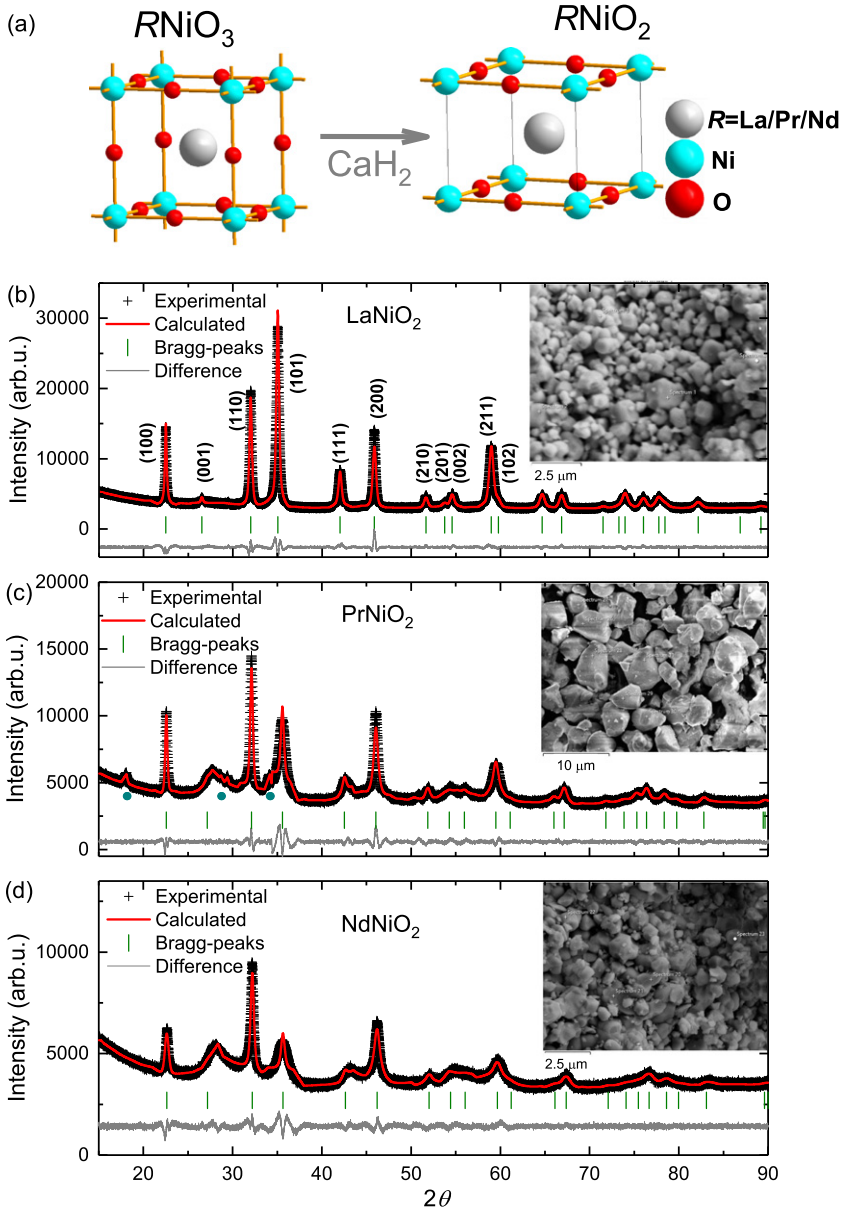

Figure 1. Schematic structures of (a) RNiO$_3$ and RNiO$_2$ (R = La, Pr, Nd). Experimental (black crosses) and calculated (red lines, via Rietveld method) powder XRD patterns of the (b) LaNiO$_2$, (c) PrNiO$_2$ and (d) NdNiO$_2$ polycrystalline samples are shown, together with the Bragg peak positions (vertical green lines). The green dots represent the peaks from residual Ca(OH)$_2$. The insets display the respective SEM pictures.

To illustrate the anisotropic widths of the Bragg reflections in RNiO$_2$, the three main reflection classes $\langle 100\rangle$, $\langle 110\rangle$, $\langle 101\rangle$ are chosen and the corresponding full-widths at half-maximum (FWHM) of the corresponding XRD peaks are presented in table 1. It can be seen that the sharper reflections are those from diffraction planes $\langle hk0\rangle$, while the broad peaks belong to the class where l has a non-zero value. In other words, the coherent domains along the [001] direction are smaller than along [100]. This anisotropic shrinking of the crystalline size after topotactic reduction has already been observed in previous studies on nickelates [5, 6, 17, 31, 34, 37] and cobaltates [38], and are characteristic for systems with anisotropic particle size, stacking disorder, or uniaxial strain in layered compounds. In the RNiO$_2$ system, this anisotropy may be due to the stronger intra-layer than inter-layer bonding, making the structure to more likely break up along the [001] direction. On the other hand, the crystalline sizes become smaller from LaNiO$_2$, PrNiO$_2$ to NdNiO$_2$, especially for $\langle 101\rangle$. This indicates an increasing instability of the RNiO$_2$ structure from R = La, Pr to Nd, which could be caused by the smaller lattice parameters and consequently the stronger inter-layer Ni–Ni interactions. This would be consistent with previous research on Nd$_{1-x}$Sr$_x$NiO$_2$ where a higher Sr-doping level with a larger c-axis parameter exhibits a sharper and more intense $\langle 101\rangle$ peak [5, 6].

Table 1. Systematic comparison between RNiO$_2$ (R = La, Pr, Nd) and $Pr_4Ni_3O_8$ [39].

Compound	$LaNiO_2$	$PrNiO_2$	$NdNiO_2$	$Pr_4Ni_3O_8$
R^{3+} configuration	$4f^0$	$4f^2$	$4f^3$	
a at 300 K (Å)	3.9582(1)	3.9403(3)	3.9279(4)	
c at 300 K (Å)	3.3632(3)	3.2845(8)	3.2793(11)	
a/c at 300 K	1.18	1.20	1.20	
R_p (%)	2.1	2.1	1.9	
R_{wp} (%)	3.0	3.4	2.6	
FWHM⟨100⟩ (°)	0.21	0.23	0.29	
FWHM⟨110⟩ (°)	0.28	0.31	0.38	
FWHM⟨101⟩ (°)	0.41	0.87	1.03	
T_p at 0.02 T (K)	11.8	6.7	4.8	
δ	0.077	0.049	0.064	0.057
τ_* (s)	2.8×10^{-5}	2.7×10^{-6}	1.9×10^{-6}	$\sim10^{-6}$
T_s (K)	11.4	8.7	5.1	68.3
$z\nu$	3.7	4.2	5.2	3.8
τ_0 (s)	1.7×10^{-5}	6.7×10^{-6}	1.3×10^{-6}	$\sim10^{-6}$
T_0 (K)	9.7	7.8	4.4	60.1
E_a/k_B (K)	26.1	15.9	15.2	130
τ_r (s)	1.4×10^{3}	1.4×10^{3}	1.6×10^{3}	1.8×10^{3}
β	0.49	0.47	0.45	0.49

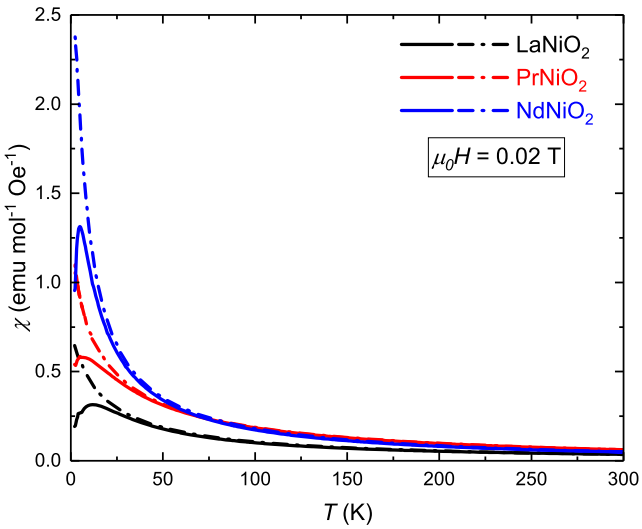

Figure 2. DC magnetic susceptibilities at 0.02 T for $LaNiO_2$ (black), $PrNiO_2$ (red) and $NdNiO_2$ (blue), respectively. The solid lines are measured for zero-field cooling (ZFC) and the dashed ones for field cooling (FC) processes.

It is worth noting that there are no observable nickel impurities in these samples. The nickel was one of the prime suspects responsible for the FM-like transition at low temperature as well as the weak magnetic hysteresis in bulk $Nd_{0.8}Sr_{0.2}NiO_2$ and $Sm_{0.8}Sr_{0.2}NiO_2$ [5–7]. To further exclude the possibility of nickel impurities, we re-oxidized the samples back to RNiO$_3$ and did not observe any NiO. In addition, we measured the nickel powders synthesized using the same method and did not find any frequency-dependent behaviour as we describe below. Combining all of this evidence, we may claim to have no observable amount of crystalline nickel impurities in the as-synthesized $LaNiO_2$, $PrNiO_2$ and $NdNiO_2$ samples, and the magnetic measurements to be presented below reveal intrinsic properties of these poly-crystalline samples. The broad feature around $2\theta = 28°$ for $PrNiO_2$ and $NdNiO_2$ of unknown origin which also occurs in the corresponding data of other works [5, 17, 21] is not likely to affect this result, as the $LaNiO_2$ without this feature still show a similar magnetic behaviour.

The DC magnetic susceptibilities $\chi(T)$ under a magnetic field of 0.02 T for the RNiO$_2$ samples (R = La, Pr, Nd) are shown in figure 2. It is obvious that there are peak-like structures at 11.8 K for $LaNiO_2$, 6.7 K for $PrNiO_2$ and 4.8 K for $NdNiO_2$, respectively. Taking into account of the huge difference between ZFC and FC data above the peak temperature, we interpret this peak-like temperature as a spin-glass

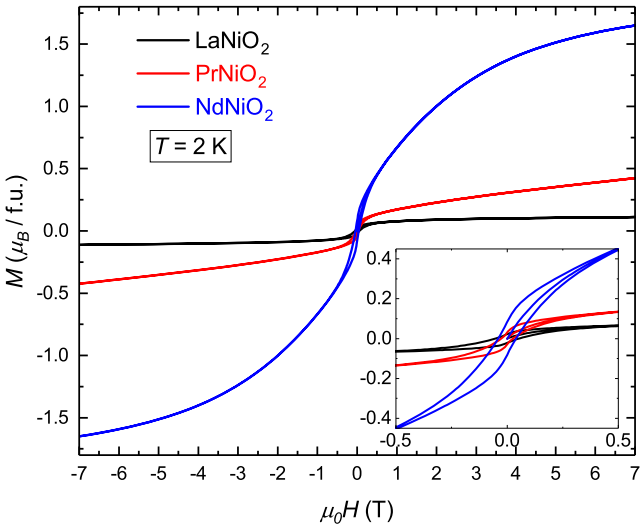

Figure 3. Magnetic-hysteresis loops at 2 K for RNiO$_2$ (R = La, Pr, Nd). The inset is the enlarged view for low magnetic fields.

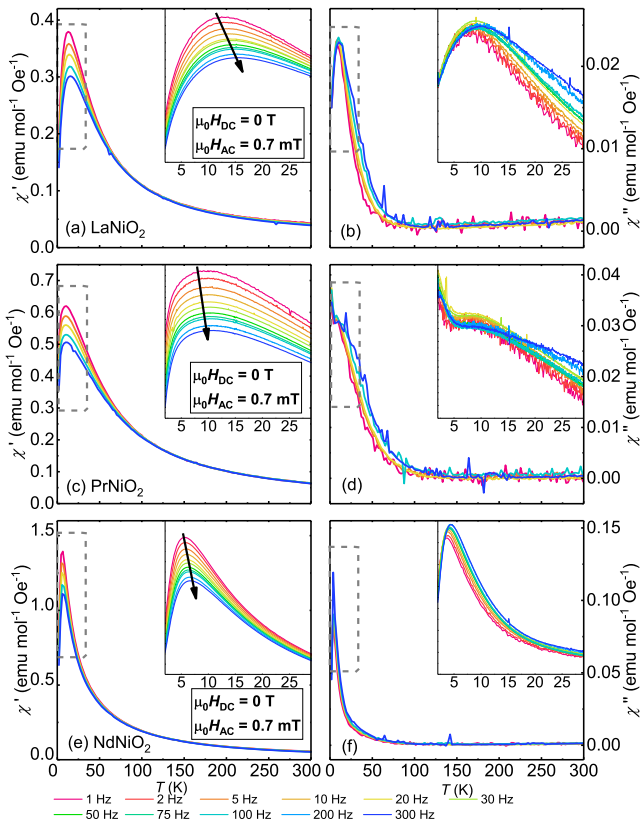

Figure 4. Real part χ' and imaginary part χ'' of the AC magnetic susceptibility of RNiO$_2$ (R = La, Pr, Nd) measured at different frequencies with zero external DC magnetic field. The insets are enlarged drawings from 2 K to 30 K. The black arrows illustrate the shifts of the χ' peak temperatures T_p.

freezing process, and the corresponding peak temperature is in fact a spin freezing temperature T_f. The weak hysteresis shown in figure 3 in bulk RNiO$_2$ samples can also be considered as a feature of a spin-glass state.

The AC susceptibility technique can be used as a probe of magnetic dynamics to distinguish spin-glass systems from other, long-range ordered systems [40]. The results of systematic AC susceptibility measurements on RNiO$_2$ (R = La, Pr, Nd) samples for AC frequencies ranging from 1 Hz to 300 Hz are plotted in figure 4. The applied DC magnetic field is 0, and the AC magnetic fields have the same amplitude of 0.7 mT. In all cases, we observe distinct peaks in the real parts χ' of the magnetic susceptibility, and an

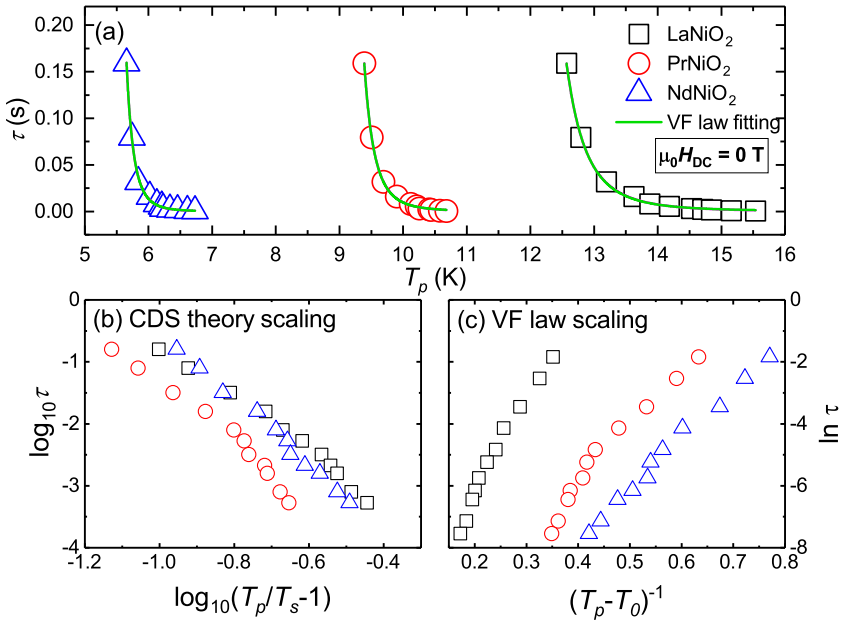

Figure 5. (a) Measured oscillation periods $\tau = (2\pi f)^{-1}$ as functions of peak temperatures T_p of the AC χ' curves for $LaNiO_2$ (black squares), $PrNiO_2$ (red circles) and $NdNiO_2$ (blue triangles). The green lines present the fitting results by VF laws. The scaling plots, corresponding to critical dynamical scaling (CDS) theory and Vogel–Fulcher (VF) laws are shown in (b) as $\log_{10}\tau \sim \log_{10}(T_p/T_s - 1)$ and (c) as $\ln\tau \sim (T_p - T_0)^{-1}$, respectively.

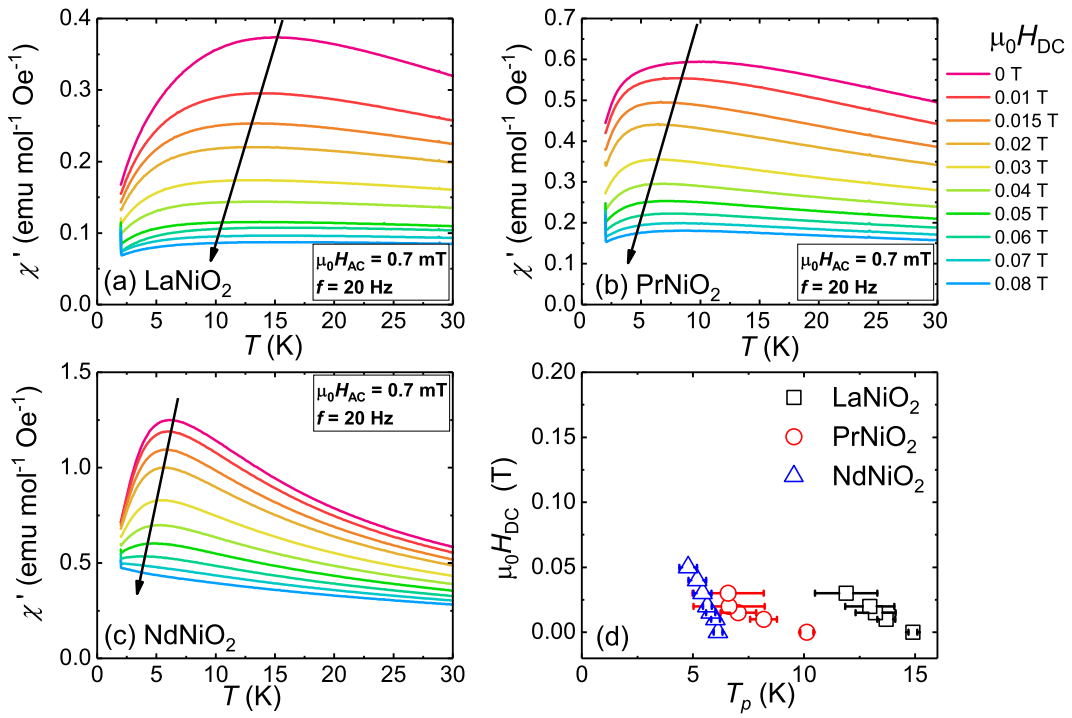

Figure 6. Real part $\chi'(T)$ of the AC magnetic susceptibility of (a) $LaNiO_2$, (b) $PrNiO_2$ and (c) $NdNiO_2$ measured in different external DC magnetic fields from 0 to 0.08 T. (d) Peak temperature T_p of $RNiO_2$ as a function of H. Due to the magnetic field broadening of the peaks in $\chi'(T)$, the T_p for $\mu_0 H_{DC} > 0.05$ T cannot be determined very accurately (see error bars).

upward shift of the peak temperatures with increasing frequency f. At the same time, the imaginary parts χ'' indicate strong dissipation starting already below ~100 K, with a maximum around the peak temperatures of the respective χ' data, with the exception of $PrNiO_2$ where the peak structure in χ'' is less clear. Such a behaviour is characteristic of spin-glass systems and distinguishes them from disordered AFM systems, in which χ'' remains zero even below the transition temperature [41–43]. Apart from these, however, there is

an intriguing deviation from the typical spin-glass behaviour: the frequency-dependence disappears only at temperatures as high as 70–100 K, nearly 10 times higher than the peak temperature. This may indicate a complex magnetism in $R\mathrm{NiO_2}$, similar to that we have reported for the square planar nickelate $\mathrm{Pr_4Ni_3O_8}$ [39]. Multiple magnetic disorders may participate in the frustration of magnetic interactions, one that is dominating the freezing process at T_p, accompanied by another, more gradual one at a higher temperature. Interestingly, this temperature region is close to the metal–insulator transition temperature observed in the electric resistivities of $R\mathrm{NiO_2}$ thin films [1, 2, 44]. This may imply an underlying relationship between the magnetic disorder and insulating behaviour.

The relative variation of the freezing temperature T_f per frequency decade $\delta = \Delta T_\mathrm{f}/\left(T_\mathrm{f}\Delta \log_{10} f\right)$, is often employed as a parameter to compare different kinds of spin-glass systems. It reflects the strength of magnetic interactions between the underlying entities. Here, the peak temperature T_p is identified as the spin glass freezing temperature T_f. The values of δ obtained in this way are all very close, namely 0.077, 0.049, and 0.064 for $\mathrm{LaNiO_2}$, $\mathrm{PrNiO_2}$ and $\mathrm{NdNiO_2}$, respectively. These values are intermediate between canonical spin-glass systems such as CuMn [45] ($\delta = 0.005$) and superparamagnetic systems such as α-$[\mathrm{Ho_2O_3(B_2O_3)}]$ [48] ($\delta = 0.28$). They fall within the order of magnitude usually observed for cluster spin glasses, such as Ni-doped $\mathrm{La_{1.85}Sr_{0.15}CuO_4}$ [46] ($\delta = 0.012$), $\mathrm{PrRhSn_3}$ [47] ($\delta = 0.086$), and therefore $R\mathrm{NiO_2}$ resembles the case of cluster spin glasses.

To obtain a more detailed insight in the spin-glass behaviour, we have studied the relation between T_p and the fluctuation time $\tau = (2\pi f)^{-1}$, as presented in figure 5(a). The CDS theory predicts a power law:

$$\tau = \tau_* \left(\frac{T_\mathrm{p}}{T_\mathrm{s}} - 1 \right)^{-z\nu}. \tag{1}$$

In this equation, τ describes the fluctuation time scale, z the dynamic critical exponent reflecting the correlated dynamics diverging as $\tau \propto \xi^z$, and ν the static critical exponent describing the divergence of the correlation length $\xi \propto (T - T_\mathrm{s})^{-\nu}$. The τ_* is the relaxation time of a fluctuating entity flip, and $T_\mathrm{s} < T_\mathrm{p}$ is the static freezing temperature as f tends to zero. From table 1, the resulting τ_* of $R\mathrm{NiO_2}$ is 10^{-5}–10^{-6} s, far larger than the typical values for a canonical spin glass, 10^{-12}–10^{-14} s [48], and still larger than the values of the reported cluster spin-glasses 10^{-7}–10^{-10} s [46, 48]. Such a high value of τ_* implies a slow dynamics of the fluctuating entities of $R\mathrm{NiO_2}$. The resulting $z\nu$ of $R\mathrm{NiO_2}$ lies around 4–5, at the lower bound found in typical spin glass systems 4–12 [48].

Alternatively, the spin glass state can also be described by the VF law. By introducing an empirical 'true transition point or anomaly' at T_0 into the conventional Arrhenius law, the VF law can be written as

$$\tau = \tau_0 \exp\left(\frac{E_a/k_\mathrm{B}}{T_\mathrm{p} - T_0} \right). \tag{2}$$

In this equation, τ_0 is essentially equivalent to τ_* (see table 1), and E_a is an energy barrier. Considering E_a in general to be correlated with the transition temperature for different spin-glass systems, $E_a/k_\mathrm{B}T_0$ is a more meaningful measure of the coupling between the interacting entities. An $E_a/k_\mathrm{B}T_0 \gg 1$ would indicate a weak coupling, and $E_a/k_\mathrm{B}T_0 \ll 1$ a corresponding strong coupling. The value we obtain for $R\mathrm{NiO_2}$ is 2–3, in the intermediate regime. The scaling plots according to the CDS theory and the VF law are shown in figures 5(b) and (c). As neither type of representation spanning nearly three frequency decades yields a strictly linear behaviour, we cannot conclusively distinguish between the two models, however. The corresponding fitting parameters are summarized in table 1.

Furthermore, the DC magnetic field dependence of AC susceptibility χ' around the freezing temperature is shown in figure 6 for (a) $\mathrm{LaNiO_2}$, (b) $\mathrm{PrNiO_2}$ and (c) $\mathrm{NdNiO_2}$, respectively. The applied DC magnetic fields range from 0 to 0.08 T. The amplitude of AC magnetic field is 0.7 mT and the frequency is 20 Hz. One can see that the peaks in χ' are significantly suppressed with increasing DC magnetic field and may even vanish in moderately high DC magnetic fields of the order of 1 T or even less. The corresponding peak temperatures T_p, and along with them most likely also the spin freezing temperatures $T_\mathrm{f} < T_\mathrm{p}$, decrease rapidly as it is usually observed in spin glasses (see figure 6(d)) [47, 49–52]. This may explain why a recent NMR study [55] performed in $\mu_0 H = 12$ T did not reveal any signs for spin-freezing in $\mathrm{LaNiO_2}$ down to $T = 0.24$ K.

A solid evidence for the spin glass behaviour in $R\mathrm{NiO_2}$ is the memory effect in the magnetization. Memory-effect measurements were performed using two different protocols, an intermittent stop cooling process (ISC-process) and a continuous warming process (CW-process). In the first one, the sample is cooled in a magnetic field of 50 Oe from 300 K down to 1.8 K. Some intermittent stops are applied at certain temperatures. During these stops, the external field is switched off quickly and the temperature is kept constant for 5000 s while taking magnetization data simultaneously. Afterwards, the field is switched

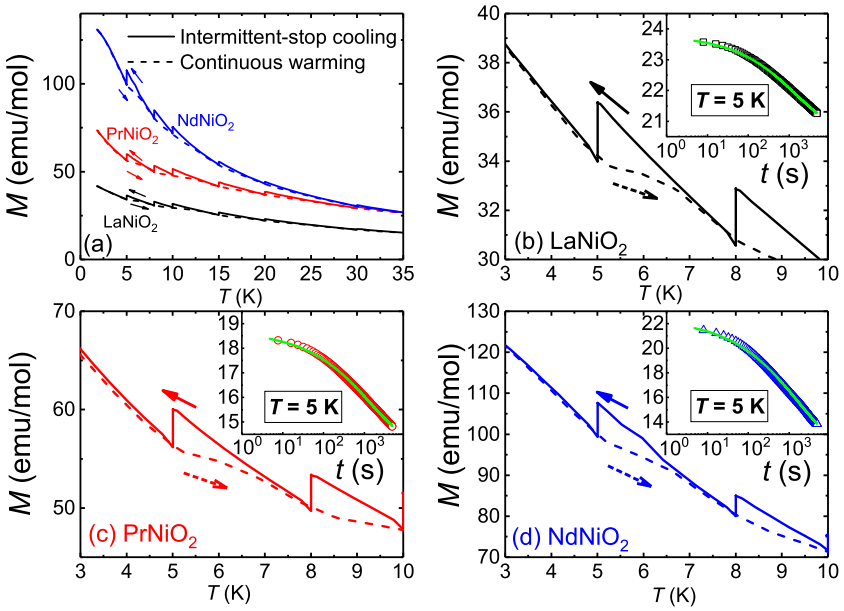

Figure 7. (a) Memory effects in RNiO$_2$ (R = La, Pr, Nd). The solid lines are measured in the intermittent-stop cooling process and the dashed ones in the continuous warming process. The enlarged views are respectively shown in (b)–(d). The insets illustrate the time evolution of magnetic susceptibility measured at 5 K, immediately after turning off the external magnetic field. And the green lines represent the fitting results by stretched exponential functions.

back to the original value and the sample further cooled down. Eventually at 1.8 K, this process is immediately followed by warming continuously from 1.8 K to 300 K. A typical feature of disordered spin glasses is a relatively long timescale to reach an equilibrium state when the magnetic field is changed. The magnetization in the glassy region would show decays in the ISC-process, and peculiar history dependent effects in the CW-process. As shown in figure 7, we can see a significant memory effect in all RNiO$_2$ compounds, in which the CW-process data (dashed lines) show distinct features at the previous stopping temperatures, and therefore reflect the history of the previous ISC-process. Another typical feature of spin glasses is that the magnetization below T_p decays slowly after the magnetic field is turned off. The insets of figures 7(b)–(d) show the magnetic moment measured at 5 K for 5000 s after setting the field to zero. The time decay of the magnetization can be fitted perfectly by a stretched exponential function,

$$M(t) = M_0 + M_g \exp\left[-\left(\frac{t}{\tau_r}\right)^{\beta}\right], \tag{3}$$

where M_0 is an intrinsic magnetization, M_g is related to a glassy component of magnetization, τ_r is the characteristic relaxation time constant, and β is the stretching exponent, which has values between 0 and 1 and is a function of temperature only. The fitting parameters τ_r and β for RNiO$_2$ and Pr$_4$Ni$_3$O$_8$ are presented in table 1, and the respective fitting results are shown as the green lines in figure 7. All these phenomena above are strongly indicative of a typical spin glass behaviour in RNiO$_2$.

It is necessary to verify that the observed spin-glass behaviour in these nickelate samples is not caused by nickel impurities. On the one hand, the structural and elemental analysis showed no crystalline nickel in the samples. On the other hand, after a complete reduction to R_2O_3 and Ni as we mentioned above for the TG experiments, the resulting products show a complete absence of spin-glass behaviour (see supplementary material (https://stacks.iop.org/NJP/24/013022/mmedia)). Even if there had been elemental nickel impurities (crystalline or amorphous) induced by the initial reduction process and mimicking a spin-glass sate in RNiO$_2$, the same feature could also be expected in the fully reduced samples.

4. Discussion

We state that bulk RNiO$_2$ samples show a universal spin glass behaviour, without any sign of long-range magnetic orders [17, 31]. This is distinct from the parent cuprates which host AFM long-range order. The fitting parameters from the spin-dynamics models are similar for all RNiO$_2$ as well as Pr$_4$Ni$_3$O$_8$ [39] (see table 1), implying the similar spin-glass nature in these nickelates. According to these results, the magnetic entities in RNiO$_2$ are expected to be cluster-like, rather than atomic single spins, and the

interaction between the entities is not weak. Within the RNiO$_2$ system itself, we find that the relaxation times τ_0 and τ_* become shorter and the energy barrier E_a smaller from R = La, Pr to Nd. It is interesting to note that while the spin-freezing temperatures T_f decrease from La, Pr to Nd, the critical temperatures in the Sr-doped thin-film versions of RNiO$_2$ increase (no superconductivity for R = La [1], and T_c = 7–12 K for R = Pr [2], and T_c = 9–15 K for R = Nd [1]). This has been attributed to a possible essential role of the 4f-electrons of the R ions, and/or to stronger interactions between the Ni $3d_{z^2}$ orbitals owing to a smaller c-axis lattice parameter [13].

One question to be clarified is whether the observed spin-glass behaviour in the bulk RNiO$_2$ systems is intrinsic or not. First, the spin-glass behaviour is not likely due to elemental Ni particles, as is stated above. Second, we may refer to the strong similarity to the spin-glass dynamics in Pr$_4$Ni$_3$O$_8$ [39] observed in very homogeneous single crystals. Given the fact that the electronic structure of the latter compound has been proposed to be very similar to that of NdNiO$_2$ [54], we may conclude that the magnetic frustration causing the universal spin-glass behaviour in bulk RNiO$_2$ and perhaps even in Pr$_4$Ni$_3$O$_8$ has a common cause, and is not due to weak crystallization. Nevertheless, the fact that T_s in the latter compound is almost one order of magnitude larger than in bulk RNiO$_2$, may hint to certain differences.

Considering that Pr$_4$Ni$_3$O$_8$ is prepared by the topotactic reduction method similar to the title compounds, we cannot entirely rule out that the spin-glass behaviour could result from local non-stoichiometries of oxygen caused by incomplete or inhomogeneous reduction. An off-stoichiometric oxygen content can alter the coordination environment, thereby lead to distributed high-valence-state Ni ions and consequently make a frustration between various magnetic interactions possible. However, taking the essential role played by the interface and strain effect in nickelate thin films [9] into account, the superconductivity along with the potential long-range magnetic order in thin films is not necessarily in contradiction to the occurrence of a disordered magnetism in bulk samples. With this respect, the spin-glass behaviour in bulk RNiO$_2$ can indeed be intrinsic. The spin glass state in RNiO$_2$ could arise from the self-doping effect of Nd 5d electron pockets [27, 56, 57]. Zhang *et al* [56], proposed NdNiO$_2$ to be a self-doped Mott insulator, where the low-density Nd 5d conduction electrons couple to the localized Ni $3d_{x^2-y^2}$ electrons to form Kondo spin singlets at low temperatures. This self-doping effect suppresses the AFM long-range order. Choi *et al* [58], proposed that the Ni $3d_{z^2}$ orbitals also participate strongly and forms a flat band pinned to the Fermi level in the nickelates. As a result, the magnetic orders are unstable and can be easily frustrated by the strong spin, charge, and lattice fluctuations, resulting in a spin disordered state but with AFM correlations [13]. Leonov *et al* [59], also proposed that an unanticipated frustration of magnetic interactions in Nd$_{1-x}$Sr$_x$NiO$_2$ suppresses magnetic order. Werner *et al* [60], argued that the optimally doped nickelate system is in a spin-freezing crossover region. Both overdoped and underdoped system are in a spin-freezing (or spin-glass-like) state, and the associated fluctuations of local moments may provide the pairing glue for the occurrence of superconductivity.

The spin-glass behaviour in the bulk infinite nickelates is partly reminiscent of that in the lightly-doped cuprates La$_{2-x}$Sr$_x$CuO$_4$ [53]. A spin-glass phase has been found at intermediate concentrations between the AFM phase and superconducting phases ($0.02 < x < 0.05$) [61]. This phase is formed by frozen AFM clusters, which have been argued to originate from the spatial charge segregation in the CuO$_2$ planes [61]. This spin-glass regime extends far into the SC state, indicating a microscopic coexistence of superconductivity and frozen AFM clusters at low temperatures [62]. As a comparison, our AC magnetic measurements reveal that the magnetic entities of nickelates are also clusters rather than single spins. Considering the fact that stripe phases have been widely observed in other layered nickelates [63–65], one may wonder if the magnetic clusters in bulk 112 nickelates indicate any internal charge segregation. Our presented data, however, do not allow to shed more light on this issue.

5. Conclusions

To conclude, we successfully synthesized bulk samples of the parent compounds RNiO$_2$ (R = La, Pr, Nd) and performed comprehensive magnetic measurements on them. The history-dependent DC magnetic susceptibilities, the magnetic hysteresis, the frequency dependence of the AC magnetizations, and more importantly, the memory effect reveal a universal spin-glass behaviour. According to phenomenological fitting results, we find that bulk RNiO$_2$ systems share a similarly slow spin dynamics as Pr$_4$Ni$_3$O$_8$, although with an almost one-order-of magnitude lower spin-freezing temperature. The magnetic entities are most probably cluster-like, and the interactions between these entities are not weak. Based on our investigations, we suggest that the universal spin glass behaviour in bulk RNiO$_2$ may be due to off-stoichiometric oxygen or even to an intrinsic magnetic frustration, rather than to impurities or weak crystallization.

Acknowledgments

This work was supported by the Swiss National Foundation under Grants Nos. 20-175554, 206021-150784.

Data availability statement

All data that support the findings of this study are included within the article (and any supplementary files).

ORCID iDs

Hai Lin https://orcid.org/0000-0002-6139-4563
Dariusz Jakub Gawryluk https://orcid.org/0000-0003-4460-7106
Ekaterina Pomjakushina https://orcid.org/0000-0002-2446-3830
Andreas Schilling https://orcid.org/0000-0002-3898-2498

References

[1] Li D, Lee K, Wang B Y, Osada M, Crossley S, Lee H R, Cui Y, Hikita Y and Hwang H Y 2019 *Nature* **572** 624
[2] Osada M *et al* 2020 *Nano Lett.* **20** 5735–40
[3] Osada M, Wang B Y, Goodge B H, Harvey S P, Lee K, Li D, Kourkoutis L F and Hwang H Y 2021 arXiv:2105.13494
[4] Zeng S W *et al* 2021 arXiv:2105.13492
[5] Li Q, He C, Si J, Zhu X, Zhang Y and Wen H-H 2020 *Commun. Mater.* **1** 16
[6] Wang B *et al* 2020 *Phys. Rev. Mater.* **4** 084409
[7] He C, Ming X, Li Q, Zhu X, Si J and Wen H-H 2020 arXiv:2010.11777
[8] He R, Jiang P, Lu Y, Song Y, Chen M, Jin M, Shui L and Zhong Z 2020 *Phys. Rev.* B **102** 035118
[9] Zeng S W *et al* 2021 arXiv:2104.14195
[10] Wu X, Jiang K, Di Sante D, Hanke W, Schnyder A P, Hu J and Thomale R 2020 arXiv:2008.06009
[11] Zhang Y, Lin L-F, Hu W, Moreo A, Dong S and Dagotto E 2020 *Phys. Rev.* B **102** 195117
[12] Leonov I and Savrasov S Y 2020 arXiv:2006.05295
[13] Pickett W E 2020 *Nat. Rev. Phys.* **3** 7–8
[14] Hu W *et al* 2020 *Phys. Rev.* B **101** 220510(R)
[15] Leca V, Blank D H A, Rijnders G, Bals S, van Tendeloo G and Salluzzo M 2006 *Appl. Phys. Lett.* **89** 092504
[16] Krockenberger Y, Ikeda A, Kumakura K and Yamamoto H 2018 *J. Appl. Phys.* **124** 073905
[17] Hayward M A and Rosseinsky M J 2003 *Solid State Sci.* **5** 839–50
[18] Li D, Wang B Y, Lee K, Harvey S P, Osada M, Goodge B H, Kourkoutis L F and Hwang H Y 2020 *Phys. Rev. Lett.* **125** 027001
[19] Zeng S *et al* 2020 *Phys. Rev. Lett.* **125** 147003
[20] Siegrist T, Zahurak S M, Murphy D W and Roth R S 1988 *Nature* **334** 231
[21] Fu Y *et al* 2020 arXiv:1911.03177
[22] Hepting M *et al* 2020 *Nat. Mater.* **19** 381–5
[23] Lee K-W and Pickett W E 2004 *Phys. Rev.* B **70** 165109
[24] Botana A S and Norman M R 2020 *Phys. Rev.* X **10** 011024
[25] Norman M R 2020 *Physics* **13** 85
[26] Jiang M, Berciu M and Sawatzky G A 2020 *Phys. Rev. Lett.* **124** 207004
[27] Gu Y, Zhu S, Wang X, Hu J and Chen H 2020 *Commun. Phys.* **3** 84
[28] Choi M-Y, Lee K-W and Pickett W E 2020 *Phys. Rev.* B **101** 020503(R)
[29] Bandyopadhyay S, Adhikary P, Das T, Dasgupta I and Saha-Dasgupta T 2020 *Phys. Rev.* B **102** 220502
[30] Zhang R, Lane C, Singh B, Nokelainen J, Barbiellini B, Markiewicz R S, Bansil A and Sun J 2020 arXiv:2009.05816
[31] Hayward M A, Green M A, Rosseinsky M J and Sloan J 1999 *J. Am. Chem. Soc.* **121** 8843
[32] Gawryluk D J *et al* 2019 *Phys. Rev.* B **100** 205137
[33] Rietveld H M 1969 *J. Appl. Crystallogr.* **2** 65–71
[34] Crespin M, Isnard O, Dubois F, Choisnet J and Odier P 2005 *J. Solid State Chem.* **178** 1326–34
[35] Crespin M, Levitz P and Gatineau L 1983 *J. Chem. Soc. Faraday Trans.* **2** 1181–94
[36] Jia Y Q 1991 *J. Solid State Chem.* **95** 184–7
[37] Retoux R, Rodriguez-Carvajal J and Lacorre P 1998 *J. Solid State Chem.* **140** 307
[38] Hayward M A and Rosseinsky M J 2000 *Chem. Mater.* **12** 2182–95
[39] Huangfu S, Guguchia Z, Cheptiakov D, Zhang X, Luetkens H, Gawryluk D J, Shang T, von Rohr F O and Schilling A 2020 *Phys. Rev.* B **102** 054423
[40] Topping C V and Blundell S J 2019 *J. Phys.: Condens. Matter* **31** 013001
[41] Körner S, Weber A, Hemberger J, Scheidt E-W and Stewart G R 2000 *J. Low Temp. Phys.* **121** 105
[42] Süllow S, Nieuwenhuys G J, Menovsky A A, Mydosh J A, Mentink S A M, Mason T E and Buyers W J L 1997 *Phys. Rev. Lett.* **78** 354
[43] Mulder C A M, van Duyneveldt A J and Mydosh J A 1982 *Phys. Rev.* B **25** 515(R)
[44] Ikeda A, Krockenberger Y, Irie H, Naito M and Yamamoto H 2016 *Appl. Phys. Express* **9** 061101
[45] Mulder C A M, van Duyneveldt A J and Mydosh J A 1981 *Phys. Rev.* B **23** 1384
[46] Malinowski A, Bezusyy V L, Minikayev R, Dziawa P, Syryanyy Y and Sawicki M 2011 *Phys. Rev.* B **84** 024409
[47] Anand V K, Adroja D T and Hillier A D 2012 *Phys. Rev.* B **85** 014418
[48] Mydosh J A 1993 *Spin Glasses: An Experimental Introduction* (London: Taylor and Francis)
[49] Kundu S and Nath T K 2012 *J. Appl. Phys.* **111** 113903

[50] Wang F, Kim J, Kim Y-J and Gu G D 2009 *Phys. Rev.* B **80** 024419
[51] Kumar A, Tandon R P and Awana V P S 2011 *J. Appl. Phys.* **110** 043926
[52] Bag P, Baral P R and Nath R 2018 *Phys. Rev.* B **98** 144436
[53] Chou F C, Belk N R, Kastner M A and Birgeneau R J 1995 *Phys. Rev. Lett.* **75** 11
[54] Karp J, Hampel A, Zingl M, Botana A S, Park H, Norman M R and Millis A J 2020 *Phys. Rev.* B **102** 245130
[55] Zhao D *et al* 2021 arXiv:2104.11187
[56] Zhang G M, Yang Y and Zhang F-C 2020 *Phys. Rev.* B **101** 020501(R)
[57] Zhang H, Jin L, Wang S, Xi B, Shi X, Ye F and Mei J-W 2020 *Phys. Rev. Res.* **2** 013214
[58] Choi M-Y, Pickett W E and Lee K-W 2020 *Phys. Rev. Res.* **2** 033445
[59] Leonov I, Skornyakov S L and Savrasov S Y 2020 *Phys. Rev.* B **101** 241108(R)
[60] Werner P and Hoshino S 2020 *Phys. Rev.* B **101** 041104(R)
[61] Julien M-H, Borsa F, Carretta P, Horvatić M, Berthier C and Lin C T 1999 *Phys. Rev. Lett.* **83** 604
[62] Niedermayer C, Bernhard C, Blasius T, Golnik A, Moodenbaugh A and Budnick J I 1998 *Phys. Rev. Lett.* **80** 3843
[63] Wochner P, Tranquada J M, Buttrey D J and Sachan V 1998 *Phys. Rev.* B **57** 1066
[64] Zhang J, Chen Y-S, Phelan D, Zheng H, Norman M R and Mitchell J F 2016 *Proc. Natl Acad. Sci. USA* **113** 8945
[65] Zhang J *et al* 2019 *Phys. Rev. Lett.* **122** 247201